THE JOURNAL OF BIOLOGICAL CHEMISTRY VOL. 288, NO. 30, pp. 22042–22056, July 26, 2013

Diaminothiazoles Modify Tau Phosphorylation and Improve the Tauopathy in Mouse Models*◆

Received for publication, November 15, 2012, and in revised form, May 31, 2013 Published, JBC Papers in Press, June 4, 2013, DOI 10.1074/jbc.M112.436402

Xuemei Zhang[‡1], Israel Hernandez[‡1], Damien Rei[§], Waltraud Mair[¶], Joydev K. Laha[‖], Madison E. Cornwell[‡], Gregory D. Cuny[‖], Li-Huei Tsai[§2], Judith A. J. Steen[¶], and Kenneth S. Kosik[‡3]

From the [‡]Neuroscience Research Institute, Department of Molecular, Cellular, and Developmental Biology, University of California at Santa Barbara, Santa Barbara, California 93106, the [§]Department of Brain and Cognitive Sciences, Picower Institute for Learning and Memory, Howard Hughes Medical Institute, Massachusetts Institute of Technology, Cambridge, Massachusetts 02139, the [¶]F. M. Kirby Neurobiology Center, Children's Hospital Boston and Harvard Medical School, Boston, Massachusetts 02115, the [‖]Laboratory for Drug Discovery in Neurodegeneration, Harvard NeuroDiscovery Center, Brigham and Women's Hospital and Harvard Medical School, Cambridge, Massachusetts 02139

Background: Tau is hyperphosphorylated in the tauopathies. Targeting Tau kinases CDK5 and GSK3β represents a potential therapeutic approach.
Results: Inhibitors of Tau kinases are neuroprotective, decrease PHF-1 immunoreactivity, and induce recovery of memory by fear conditioning.
Conclusion: Diaminothiazoles as CDK5 and GSK3β inhibitors improve the tauopathy in mouse models.
Significance: Dual kinase inhibition can be critical for efficacy when treating tauopathies.

Although Tau accumulation is a feature of several neurodegenerative conditions, treatment options for these conditions are nonexistent. Targeting Tau kinases represents a potential therapeutic approach. Small molecules in the diaminothiazole class are potent Tau kinase inhibitors that target CDK5 and GSK3β. Lead compounds from the series have IC_{50} values toward CDK5/p25 and GSK3β in the low nanomolar range and no observed toxicity in the therapeutic dose range. Neuronal protective effects and decreased PHF-1 immunoreactivity were observed in two animal models, 3×Tg-AD and CK-p25. Treatment nearly eliminated Sarkosyl-insoluble Tau with the most prominent effect on the phosphorylation at Ser-404. Treatment also induced the recovery of memory in a fear conditioning assay. Given the contribution of both CDK5/p25 and GSK3β to Tau phosphorylation, effective treatment of tauopathies may require dual kinase targeting.

The brains of patients with Alzheimer disease (AD)[4] undergo extensive cell death and are histopathologically characterized by both plaques containing amyloid-β protein and neurofibrillary tangles (NFTs) containing hyperphosphorylated Tau protein. Therapeutic strategies directed toward the NFTs are few and remain unproven. They include inhibition of Tau aggregation with methylene blue (1), passive Tau immunotherapy (2), microtubule stabilization (3), and inhibition of Tau kinases such as glycogen synthase kinase 3β (GSK3β) and cyclin-dependent kinase 5 (CDK5) (4–6). As a candidate target for tauopathies, CDK5 has the merit of phosphorylating Tau at NFT-associated residues. *In vitro* studies with peptide substrates indicated that a (Ser/Thr)-Pro motif directs CDK5 phosphorylation without previous phosphorylation of the substrate being required (7). Both *in vitro* Tau phosphorylation and *in vivo* transgenic mouse studies showed that CDK5 is involved in abnormal Tau phosphorylation at residues typically found phosphorylated in insoluble paired helical filament (PHF) Tau. These residues include Ser-202/Thr-205, Thr-231/Ser-235, and Ser-396/Ser-400/Ser-404 (8–10). Many of these sites can also be phosphorylated by GSK3β (11). However, GSK3β is primarily known to recognize specifically (Ser/Thr)-Pro-Xaa-Xaa-(Ser(P)) motifs, once Ser(P) has been phosphorylated by another kinase, such as CDK5. Support for developing CDK5 inhibitors also stems from its fairly specific neuronal activity due to the restricted neuronal expression of its activators p35 and p39 (12, 13). Various neuronal insults, such as oxidative stress and Aβ peptides, can cause calpain-induced cleavage of the CDK5 activator p35 to p25 (14). As a result, the membrane-targeting sequence of p35 is lost, and the CDK5-p25 complex becomes mislocalized to the cytoplasm. CDK5/p25 can induce NFTs when overexpressed in the CK-p25 mouse model, which displays distinctive neuronal loss after 6 weeks of induction preceding NFT formation (9). Also, specific inhibition of CDK5/p25 activity by overexpression of CDK5 inhibitory peptide reduced neurodegeneration *in vivo* (15). Furthermore, when CDK5 was knocked down by RNAi in the triple transgenic AD (3×Tg-AD) mouse model, NFTs were reduced (16). This model combines the expression of APP^{swe}, $PSN1^{M146v/-}$, and human P301L Tau to present an AD-like pathology that includes both Aβ plaque and NFT formation (17). Previously, we identified the small molecule diaminothiazole as a CDK5 inhibitor from high throughput screening (HTS) (18). A few

* This work was supported by National Institutes of Health Grant U01AG033931 (to K. S. K.).
◆ This article was selected as a Paper of the Week.
[1] Both authors contributed equally to this work.
[2] Investigator of the Howard Hughes Medical Institute.
[3] To whom correspondence should be addressed. E-mail: kenneth.kosik@lifesci.ucsb.edu.
[4] The abbreviations used are: AD, Alzheimer disease; NFT, neurofibrillary tangle; PHF, paired helical filament; i.c.v., intracerebroventricular; L, light; H, heavy; Aβ, amyloid β.

compounds from this series emerged from structure-activity relationship (SAR) studies as having good potency with *in vitro* IC_{50} <100 nM (19). Here, we report preclinical characterization of this diaminothiazole series of CDK5 inhibitors. Efficacy *in vivo* assays were studied in CK-p25 and 3×Tg-AD mouse models. The outcome was measured with respect to the level of phosphorylated Tau, the formation of NFTs, neuronal survival, DNA damage, and behavior. Collectively, our experiments demonstrate the neuroprotective effects of the diaminothiazole class of CDK5 inhibitor treatment compared with the controls.

EXPERIMENTAL PROCEDURES

Antibodies and Reagents

The following antibody was used: PHF-1 (1:1000; a gift from Dr. Peter Davies, Albert Einstein College of Medicine). Additional primary antibodies used included anti-CDK5 (1:500; Santa Cruz Biotechnology sc-173), anti-phosphorylated Tau Ser-235 (1:1000; Santa Cruz Biotechnology sc-181012), anti-Tau5 (1:2000; Abcam ab80579), anti-β-actin from mouse (1:1000; Sigma 5441), anti-γH2AX phospho-Ser-139 (1:1000; Abcam ab11174). Alexa 488 goat anti-rabbit IgG1 (1:5000; Molecular Probes) and Alexa 594 goat anti-mouse IgG1 (1:5000; Molecular Probes) were used as secondary fluorescent probes in histology tissue. IR-DYE 680 goat anti-mouse IgG1 (1:10,000; Odyssey) and IR-DYE 800 goat anti-rabbit IgG1 (1:5000; Odyssey) were used as secondary fluorescent probes for Western blots. Horseradish peroxidase-conjugated goat anti-mouse IgG (1:2000; Santa Cruz Biotechnology, sc2055) was also used as a secondary antibody.

All chemicals were purchased from Sigma unless specified otherwise. Polyethylene glycol 400 (PEG 400) was purchased from Fluka (81172), CellTiter 96 AQueous One Solution Cell Proliferation Assay was from Promega; protease inhibitor mixture was from Roche Applied Science (11836153001), and phosphatase inhibitor was from Thermo Scientific (78420).

Compounds

Synthesis of LDN-193594, -193665, and -212853 has been reported previously as compounds 26, 27, and 44 (19). For LDN-212828, -213842, and -213843, the diaminothiazoles were synthesized using the same approach, while the required isothiocyanates were prepared. Compound characterization by ^{1}H NMR is as follows: *LDN-213828*, ^{1}H NMR (500 MHz, DMSO-d_6) δ 1.50–1.61 (m, 6H), 3.46–3.48 (m, 4H), 6.81 (d, J = 9.0 Hz, 1H), 7.23–7.28 (m, 2H), 7.42–7. 49 (m, 2H), 7.61 (bs, 1H), 8.02–8.24 (bm, 3H), 10.45 (s, 1H); *LDN-213842,* ^{1}H NMR (500 MHz, DMSO-d_6) δ 3.38–3.41 (m, 2H), 3.68–3.70 (m, 2H), 6.86 (d, J = 11.0 Hz, 1H), 7.23–7.28 (m, 2H), 7.42–7. 49 (m, 2H), 7.71 (bs, 1H), 8.01–8.23 (bm, 3H), 10.52 (s, 1H); *LDN-213843,* ^{1}H NMR (400 MHz, DMSO-d_6) δ 3.17–3.19 (m, 2H), 3.65–3.67 (m, 2H), 6.94 (d, J = 9.2 Hz, 1H), 7.25–7.30 (m, 2H), 7.43–7. 49 (m, 2H), 7.77 (bs, 1H), 8.12–8.31 (bm, 3H), 10.60 (s, 1H).

In Vitro Experiments

CDK5 kinase activity *in vitro* assay was performed as described previously (19). The *in vitro* radioactive assay of CDK5 used H1P (histone H1-derived peptide PKTPKKAKKL) as substrate with buffer containing 20 mM MOPS, pH 7.5, 10 mM $MgCl_2$, 1 mM DTT, 0.5 mg/ml BSA. IC_{50} was determined at 40 μM H1P, 60 μM ATP, and 6.6 nM CDK5/p25 enzyme. The reactions were conducted in duplicate.

CDK5 kinase activity in primary neuronal culture was evaluated using primary cultured neurons prepared from brain hippocampus of E18 rat fetuses. The inhibition effect of the compounds on Tau phosphorylation represented by EC_{50} was evaluated by Western blot with phospho-Tau Ser-235 antibody. Anti-CDK5 was used as normalization control.

Cytotoxicity test was performed in primary neuronal culture on 24-well plates at a density of 80,000 cells/well. LD_{50} was measured after 24 h of incubation as described (18) using the CellTiter 96 AQueous One Solution Cell Proliferation Assay (Promega).

Values for *c*Log*P* and polar surface area were calculated using molinspiration. Aqueous solubility was accessed by turbidity in 1% DMSO/water solution.

Mouse microsomal stability of the compounds was determined at 10 μM using pooled male mouse liver microsomes (BD Biosciences, B6C3F1) following the manufacturer's protocols. Briefly, compounds (10 μM) were incubated (n = 2) with pooled mouse liver microsomes (0.5 mg protein/ml) at 37 °C for 0, 16, 30, 60, 120, and 240 min before termination of reactions and the compound extraction with the same volume of acetonitrile as the reaction mixture. Samples were centrifuged, and the resultant supernatant was analyzed for disappearance of parent compound by LC-UV and LC/MS/MS. The absorption under the curve was referenced to the zero time point samples (as 100%) to determine the percentage of compound remaining. The natural log plots of the percentage remaining for each compound were used to determine the half-life for the microsomal incubations. Half-life values were calculated from the relationship $t_{1/2}$ (min) = −0.693/λ, where λ was the slope of the natural logarithm of concentration to the time curve.

Animals

All experimental protocols were approved by the Institutional Animal Care and Use Committee at the University of California Santa Barbara or Massachusetts Institute of Technology in accordance with National Institutes of Health guidelines. All the triple-transgenic Alzheimer mice (3×Tg-AD, 23 months old) (17) used in this study were bred and housed at the University of California at Santa Barbara animal facility. Adult (10 weeks old) double-transgenic male CK-p25 (CamkII-tTA-TetO-p25-eGFP) mice (9) and control littermates were bred and housed at Massachusetts Institute of Technology. Mice were constantly kept under a doxycycline-supplemented diet to keep tetracycline-controlled Transcriptional Activator (tTA) inactive and block the expression of p25-eGFP. At 10 weeks of age, mice were switched and maintained on a doxycycline-free diet to turn on the expression of p25-eGFP for the following 6 weeks. p25 induction only takes place in the double CK-p25 mice carrying the two transgenes. Immunohistology and fear conditioning were done after this 6-week period of p25 induction, the time when neuronal loss and cognitive deficits are first visible (20).

Pharmacokinetics

Tissue Collection—Triple transgenic Alzheimer mice (3×Tg-AD) were i.p. injected with a single dose of LDN-193594 (120 mg/kg) dissolved in PEG 400/water (40:60, v/v). Animals were sacrificed 3, 10, 30, 60, 120, 180, and 240 min after injection. Two animals were used for each time point for pharmacokinetic analysis. Animals were anesthetized with pentobarbital (Schering-Plough); blood was collected by intracardiac puncture in 1.5-ml tubes containing EDTA, centrifuged 2500 × *g* for 10 min at 25 °C followed by 0.9% sterile saline perfusion (Baxter, USP). Plasma was obtained and stored at −80 °C until assayed. Cortex was dissected from the brain, weighed, and homogenized in 500 μl of PBS buffer, pH 7.4, and stored at −80 °C.

Sample Preparation and Analytical Methods—Analytical samples in plasma or brain homogenate were prepared by precipitation of proteins with 3 volumes of methanol. After centrifugation, the supernatant was directly submitted to LC/UV/MS analysis. Standard calibration in plasma or brain homogenate was done by diluting a series of 10× stock solutions of the compound in PEG 400/water (40:60, v/v) into either plasma or brain homogenates from untreated mouse to a 1× final concentration. Analytical methods were developed by LC/UV/MS using a Waters 2695 HPLC with a chilled autosampler connected to the Waters 996 photodiode array UV detector and micromass QTOF2 quadrupole/time-of-Flight tandem mass spectrometer. After separation on a C18 reverse phase HPLC column, Kromasil 100-5C18 (4.6 × 250 mm, 5 μm), using an acetonitrile/water gradient system, peaks were qualitatively characterized by mass spectrometry (MS/MS) using ESI ionization. Standard curves were determined based on the correlation between the concentration and UV absorption. The limit of quantification for most of the compounds tested was found to be less than 0.1 μM for both plasma and brain homogenate.

Data Analysis—A one-compartment model was used to compute pharmacokinetic values from mean compound concentration *versus* time both for plasma and brain after i.p. injection. Data were fit to a one-compartment model using the online software SBPKPD. Results are presented as mean ± S.E. of two animals for each time point (Fig. 2*A*). The brain *versus* plasma ratio was computed by dividing the brain concentration by the concurrent plasma concentration at each time point.

Ex Vivo CDK5 Kinase Assay

The assay was performed by a modified procedure described previously (16). CD1 mice (Charles River Laboratories) were euthanized 15 min after i.p. injection of LDN-193594 in 40% PEG or 40% PEG alone. According to the pharmacokinetic profile, compound LDN-193594 in the cortex reached C_{max} of 69 μM 10 min after i.p. injection. The cortex was then dissected and placed on a 1.5-ml microcentrifuge tube containing lysis buffer with protease inhibitor and phosphatase inhibitor. The tissue was homogenized, incubated for 15 min on ice, and centrifuged at 13,000 rpm at 4 °C. Supernatant was recovered in clean microcentrifuge tubes, and protein concentration was measured with the bicinchoninic acid method. CDK5 was immunoprecipitated from 250 μg of total protein using 1 μg of IgG rabbit polyclonal anti-CDK5 (C-8) antibody. IgG isotype immunoprecipitation was used as negative control and done in a parallel fashion. Antibody and protein extract were incubated overnight at 4 °C in a rotator; protein G-Sepharose was added and incubated for an additional 1 h at 23 °C, and protein G-Sepharose beads were washed five times with immunoprecipitation (IP) buffer at 4 °C. After the fifth wash, the protein G-Sepharose beads were resuspended in kinase assay buffer (20 mM MOPS, pH 7.4, 50 mM NaCl, 0.1 mM EDTA, 1 mM DTT, 10 mM $MgCl_2$), and H1 peptide was added as a substrate for CDK5 at a final concentration of 500 μM. Reaction was initiated by 4 μCi of [γ-^{32}P]ATP at a final concentration of 500 μM. The reaction mixture was incubated at 37 °C and was quenched with 5 μl of acetic acid for every 20 μl of reaction mixture at 10, 30, and 60 min. The phosphorylated H1 peptide product was separated from excess ATP by P81 cation-exchange chromatography on phosphocellulose paper using 0.1% phosphoric acid as developing solution. After complete drying at room temperature, the radioactivity of phosphorylated H1 peptide was detected by a phosphorimager and later read by a scintillation counter. For the kinase activity assay, recombinant CDK5/p25 was used as positive control, although protein fraction of IgG isotype immunoprecipitation was used as negative control. Reaction rate was calculated as the linear rate of the phosphorylated H1 peptide formation over time (μM/min).

Toxicity

3×Tg-AD (23 months old) mice were injected daily i.p. with PBS, vehicle (40–60% PEG 400), kinase inhibitors LDN-193594 (30, 60, and 120 mg/kg/day), or LDN-213828 (39 and 78 mg/kg/day). Mice were monitored for a week to determine symptoms of pain or distress, and the weight was recorded daily.

Efficacy Study

Intracerebroventricular (i.c.v.) Infusion with Ck-p25 Mouse—In the CK-p25 mouse model, the compound LDN-193594 was first delivered by i.c.v. infusion throughout the entire induction time to maximize the drug efficacy inhibiting the hyperactivation associated with p25-eGFP overexpression (Table 1, experiments 1 and 2), and the protocol was applied to LDN-213828 in experiment 3. Six-week Alzet pumps (model 2006, Alzet osmotic pumps) were filled with excipient or the experimental compound in excipient at a concentration to ensure a diffusion of 100 nmol of compound per day. Pumps were connected to an i.c.v. plunger (brain infusion kit III, Alzet osmotic pumps) through a 2-cm tube connector previously filled with the same solution. Once assembled, pumps were kept for 2 h at 37 °C in sterile saline to allow pump priming. Mice were anesthetized using a mixture of ketamine/xylazine/buprenex (100:10:0.1 mg/kg, respectively) and placed in a stereotaxic apparatus (Kopf Instruments). Pumps were placed in the inter-shoulder blade area, and the i.c.v. plunger was lowered through a surgically drilled hole in the skull to allow the placement of the plunger cannula tip at the following coordinates: anterior-posterior = −0.46, lateral −1.25 mm from Bregma, and dorsal −2.25 mm from the skull surface. Those coordinates allowed infusion of the drug in the i.c.v. space. Once the plunger was lowered to the half-distance, surgical glue was applied around

TABLE 1
Summary of drug efficacy in two mouse models
Statistical significance is indicated as follows: *, $p < 0.05$; **, $p < 0.01$, and ***, $p < 0.001$.

Mouse model	Route/compound/ excipient	Exp. no.	Dose per day	No. of mice/time of treatment	Immuno-staining PHF-1	Reversal of neuronal cell loss/DNA damage	Reduction of Tau phosphorylation
			mg/kg				
CK-p25	i.c.v. 594; DMSO 50%	1	1	7/6 weeks	50%***	62% Cell reversal***	20%*
		2	0.5	6/6 weeks	52%***	39% Cell reversal *	80%***
	i.c.v. 828; PEG 60%	3	1	3/6 weeks	51%***	22% Cell Reversal	89%***
	s.c./i.p. 594; PEG[a]	4	30/60[b]	4/3 weeks	61%***	42% cell reversal**	78%***
	s.c./i.p. 828; PEG[c]	5	30/60[b]	4/3 weeks	64%***	48% cell reversal*	85%***
3×Tg-AD	i.p. 594; 40% PEG	6	60	6/1 week	99%**	91% DNA reversal **	81%**
		7	30	6/1 week	79%**	85% DNA reversal *	68%*
	i.p. 828; 60% PEG	8	78	4/1 weeks	61%*	78% DNA reversal *	65%*
		9	39	4/1 week	95%**	99% cell reversal **	78%*
	s.c. injection 594; 40% PEG	10	60	5/1 week	32%	60% cell reversal	40%

[a] Compound LDN-193594 was administered s.c. in 100% PEG and then administered i.p. in 40% PEG, 40% saline.
[b] 30 mg/kg/day s.c. infusion was for 2 weeks, followed by 60 mg/kg/day i.p. injection on the 3rd week.
[c] Compound LDN-193828 was administered s.c. in 100% PEG and then administered i.p. in 60% PEG, 40% saline.

its base (Loctite 454, Alzet osmotic pumps) and then lowered to its final position, which ensured a tight fit against the skull surface.

Subcutaneous/Intraperitoneal (s.c./i.p.) Experiment—CK-p25 mice and control littermates with p25 induced for 3 weeks were treated with a combination of s.c. and i.p. drug delivery; at first, mice were subcutaneously implanted with 2-week osmotic pumps (Alzet, model 2004) filled with a solution of excipient or compound in excipient so mice would receive a treatment for 2 weeks at 1× dose. Then, for the last week of p25 induction, mice received daily i.p. delivery of the same solution at 2× dose. Mice were then sacrificed, and the effect of the treatment on neuron loss and Tau phosphorylation was evaluated. CK-p25 mice already induced for 3 weeks were treated with s.c. infusion of 30 mg/kg/day in the following 2 weeks and with a daily i.p. injection of 60 mg/kg during the 6th week of p25 overexpression (experiment 4). We did not analyze the concentration reached in the brain following this treatment but noticed some of the compound had precipitated in the area around the pump implantation site. This slight precipitation seemed to indicate that C_{max} in the infusion delivery was reached and that prompted us to combine this treatment with daily i.p. injections, which allowed a larger volume and higher concentration for drug administration, during the last week of treatment. LDN-213828 was delivered according to the same protocol (experiment 5). Based on its molecular weight, the doses were 39 and 78 mg/kg/day s.c. and i.p., respectively. We chose to treat the 3×Tg-AD daily for 1 week via i.p. injection with compound LDN-193594 in two doses (30 and 60 mg/kg/day) (experiments 6 and 7). The same protocol was applied to compound LDN-213828 in experiments 8 and 9. Finally, we delivered compound LDN-193594 at 60 mg/kg/day by s.c. injection in experiment 10. After treatment, all mice were anesthetized, followed by intracardiac perfusion with 0.9% sterile saline solution (Baxter, USP). The brain was removed and hemilaterally excised. The left hemisphere was subsequently used for immunofluorescence, whereas the right hemisphere was used for immunoblotting.

Behavior

As described previously (20), fear conditioning was conducted using 6-week CK-p25-induced mice or single transgenic control littermates treated with s.c./i.p. treatment with either LDN-193594 or vehicle during the last 3 weeks of induction. The observer was blinded to the genotype and type of treatment. Mice were put in the conditioning chamber (TSE Systems) for 3 min, after which a cue phase started with a series of 4.5 kHz tone pips (250 ms on and 750 ms off) for 28 s followed by a one-time 2-s footshock (0.8 mA). Animals were then left in the box for another 30 s before being returned to their home cage. 24 h later, contextual fear-conditioning memory was measured; mice were placed back into the fear conditioning box, and contextual freezing behavior was scored during 3 min. Freezing was defined as a lack of movement, except for heartbeat and respiration, associated with a crouching posture and was recorded every 10 s for 3 min (for a total of 18 sampling intervals). The number of observations indicating freezing obtained as a mean was expressed as a percentage of the total number of observations.

Western Blot

The right cortex and hippocampus were dissected, and the tissue was weighed and homogenized in RIPA buffer containing protease and phosphatase inhibitors. Brain homogenates were then centrifuged at 20,000 × *g* for 10 min at 4 °C, and supernatant was stored at −80 °C until use. Protein lysates were quantified with bicinchoninic acid (BCA) assay (Pierce), separated in SDS, 10% PAGE at 120 V for 2 h, and transferred to nitrocellulose membranes. After incubating with primary antibodies, membranes were blotted using IR-DYE 680 anti-mouse or IR-DYE 800 anti-rabbit and detected with a LI-COR scanner (Odyssey). Densitometry of bands was measured using ImageJ software (21) and normalized to β-actin or GAPDH.

Immunohistology

The left hemisphere of the mouse brain was post-fixed for 1 week in 4% paraformaldehyde/PBS buffer and coronally sectioned using a vibratome (Leica 1000), at a thickness of 50 μm for the 3×Tg-AD mice and 40 μm for the CK-p25 mice. Four brain slices were selected from each animal, at regular intervals and spanning the anterior to posterior portions of the hippocampus. For the PHF-1 and γH2AX staining, slices were treated with 50 mM NH_4Cl for 10 min at RT, preincubated with 0.1% Triton X-100, 1% BSA, PBS for 1 h. Sections were double-

stained by incubation with PHF-1 and γH2AX antibodies at 4 °C for 3 days; Alexa 488 anti-rabbit and Alexa 594 anti-mouse were used as secondary fluorescent probes and incubated an additional day in the presence of Hoechst 33342 (Calbiochem) to fluorescently label cell nuclei. Slices were mounted in microscopy glass slices using FluorSave mounting media (Calbiochem). The same procedure was applied for NeuN and PHF-1 staining in CK-p25 mice except that NH_4Cl treatment was omitted. Staining for Fluoro-Jade (Millipore AG310) was performed following the manufacturer's recommendation except on the first step of immersion in which slices were immersed in 100% alcohol only. Confocal micrographs for hippocampal CA1 neurons immunostained with PHF-1 and γH2AX or NeuN and PHF-1 were taken. Neurons visibly stained by either PHF-1 and/or γH2AX foci were observed, manually classified using BioView software (22), and counts for classified neurons obtained.

Sarkosyl Fractionation of Tau—Sarkosyl fractionation was performed as described previously (23). Briefly, mouse hippocampi from 3×Tg-AD mice stored in RIPA buffer (50 mM Tris-HCl, pH 7.4, 150 mM NaCl, 1% Nonidet P-40, 0.5% sodium deoxycholate, 0.1% SDS) with protease and phosphatase inhibitor were diluted with Sarkosyl buffer (50 mM Tris-HCl, pH 7.4, 150 mM NaCl, 1% Sarkosyl) to 1 ml, incubated head-over-head at 4 °C for 30 min, and pre-centrifuged at 20,000 rpm for 10 min at 4 °C. The supernatant was ultracentrifuged at 200,000 rpm at 4 °C for 2 h to pellet the Sarkosyl-insoluble fraction. After removal of the supernatant, the pellet was dissolved by boiling in Laemmli buffer (Bio-Rad) plus 20 mM DTT (Sigma) at 95 °C for 10 min, separated by SDS-PAGE, immunoblotted, and subjected to sample preparation for mass spectrometric (MS) analysis.

Statistical Analysis—Statistical evaluation was performed using Student's *t* test (for two treatment comparisons) or one-way analysis of variance followed by Tukey's post hoc analysis (for multiple treatments comparisons). R project for statistical computing was used to compute statistical tests (version 2.13; R development core team, 2011). Statistical difference was considered significant at $p < 0.05$. For contextual fear conditioning, statistical evaluation was performed using one-way analysis of variance with Bonferroni's multiple post hoc test.

Mass Spectrometry—For absolute quantification and determination of PHF-Tau and its diverse phosphorylation, we used FLEXIQuant, a mass spectrometry approach that is based on the addition of a full-length protein standard containing the N-terminally tagged artificial tryptic FLEX-peptide into the biological sample of interest (24). The FLEX-peptide absolute quantity is predetermined from which the isotopically labeled FLEX-Tau^H is quantified based on its ratio to the FLEX-peptide and is used as an internal reference to quantify the endogenous Tau^L based on its L/H ratio. As the 3×Tg-AD mouse model expresses the human 4R0N isoform of Tau, we prepared the isotopically labeled FLEX-Tau^H by subcloning the longer Tau isoform human 4R1N Tau into the FLEX-peptide containing expression vector. After wheat germ expression and His tag purification, isotopically labeled [$^{13}C_6$]Lys and [$^{13}C_6$]Arg Tau standards (FLEX-Tau^H) were in-gel digested by trypsin.

Protein lysates from one-quarter of each hippocampus were Sarkosyl-extracted to enrich for PHF-Tau. The Sarkosyl-insoluble pellet was separated via SDS-PAGE and probed with PHF-1 antibody to confirm enrichment of PHF-Tau at 65 kDa. A similar gel prepared in parallel was Coomassie-stained, and gel segments corresponding to a molecular mass of ~65 kDa were excised from both vehicle and LDN-193594-treated samples. These gel segments were subjected to in-gel trypsin digestion. As Western blotting indicated large differences in PHF-Tau levels in these samples, an appropriate amount of FLEX-Tau^H was added into the sample to ensure an approximate 1:1 light to heavy (L/H) ratio of Tau peptides within the subsequent MS analysis. In the MS analysis, the nonlabeled version of the FLEX-peptide (TENLYFQGDISR) was added to the L/H peptide mix at a concentration of 10 fmol/μl (three technical repeats). To produce a heavily labeled FLEX-Tau protein standard (FLEX-Tau^H) with an N-terminal His_6 tag and the FLEX-peptide (TENLYFQGDISR), full-length human 4R1N Tau (gi:294862254) was subcloned into the previously generated pEU-E01-TEV-N1-AQUA vector (24). After the WGE translation reaction, FLEX-Tau^H was batch-purified using nickel-Sepharose beads (nickel-Sepharose high performance resin, GE Healthcare).

RESULTS

Diaminothiazoles, a Novel CDK5 Inhibitor Series—We described previously a series of diaminothiazole compounds that inhibit CDK5 within the nanomolar range. LDN-193594 (compound 26 in Ref. 19) shows an *in vitro* IC_{50} of 30 nM and EC_{50} of 5.5 μM when evaluated in rat primary neuronal cultures. To test the biological stability of LDN-193594, we incubated it with microsomes for 1 h. Using LC/MS/MS, we estimated that its half-life is ~30 min. This relatively short half-life suggested that LDN-193594 might be a substrate of CYP_{450} oxidation. To track down the putative oxidation site without purifying all the metabolites, the fragmentation pattern of the product generated by mass spectrometry was carefully examined. One of the major metabolites in the fragmentation pattern clearly suggested that an oxygen atom had been added to the pyridine, because an increase of 16 Da in the mass of the fragment was observed (data not shown). Given these data, a molecule with trifluoromethyl to block the 6-position of the 3-pyridine was synthesized (LDN-212853); this molecule exhibited an extended half-life (Fig. 1). Additional derivatives of this series were synthesized by introducing hydrophilic groups, such as piperidine, morpholine, and piperazine, at the 6-position of the 3-pyridine. The synthesized compounds were analyzed for their ability to inhibit CDK5 via an *in vitro* kinase assay and in primary neuronal cultures. As shown in Fig. 1, LDN-193665 has the higher potency in primary cultures and LDN-193594 *in vitro*. The inhibition potency decreased, as reflected by EC_{50} and IC_{50}, whereas microsome stability improved, *i.e.* LDN-213828 has the longest half-life in microsomes, about three times that of LDN-193594. All compounds selected for further testing have an LD_{50} greater than 100 μM, about 8-fold greater than the EC_{50} of LDN-213828.

To establish a drug delivery protocol that is suitable for efficacy testing in animals, we studied possible formulations of this

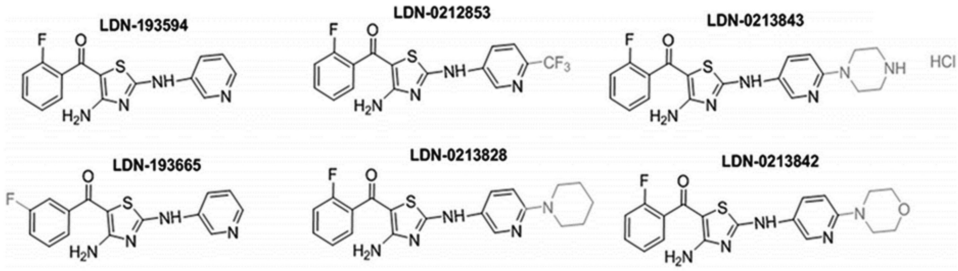

LDN#	CDK5 IC_{50}[a] (nM)	GSK3β IC_{50}[a] (nM)	EC_{50}[b] (μM)	LD_{50}[c] (μM)	microsomal stability[d] $t_{1/2}$ (min)	Aqueous Solubility (μM)[e]	PEG-400 Solubility mg/mL (mM)[e]	40%PEG-400 Solubility mg/mL (mM)	cLogP[f]	PSA (Å^2)[f]
193594	30	45	5.5	>100	31	>20	63 (200)	12 (40)	3.3	81
193665	62	19	2.8	>100	29	12	63 (200)	3.1 (10)	3.3	81
212853	160	100	7.0	>100	66	>20	38 (100)	3.8 (10)	4.3	81
213828	240	240	12.8	>100	90	>20	78 (200)	7.8 (20)[g]	4.7	84
213842	100	94	-	>100	-	>100	20 (50)	2.0 (5.0)	3.6	93
213843	90	38	6.2	>100	70	>1000	40 (92)	16 (37)	3.1	96

FIGURE 1. **Structure and chemical and biological properties of diaminothiazole.** *a*, IC_{50} for CDK5 was determined on 40 μM histone H1-derived peptide PKTPKKAKKL (H1P), 60 μM ATP, and 6.6 nM Cdk5/p25 enzyme; IC_{50} for GSK3β was determined on 40 μM glycogen synthase peptide-2 (GSP-2), 60 μM ATP, and 55 nM GSK3β. *b*, CDK5 kinase activity in primary neuronal culture was evaluated using neuronal primary culture prepared from brain hippocampus of E18 rat fetuses. *c*, LD_{50} was measured after 24 h of incubation as described previously (18) using the CellTiter® 96 AQueous One Solution Cell Proliferation Assay (Promega). *d*, mouse microsome stability of the compounds was decided at 10 μM using pooled male mouse liver microsomes (BD Biosciences, B6C3F1). The reaction mixture was analyzed using HPLC-UV method. *e*, solubility was accessed by turbidity. *f*, values for cLog*P* and polar surface area were calculated using molinspiration. *g*, 60% PEG 400 was used.

series of compounds. The excipient PEG 400 greatly improved the solubility of all compounds (Fig. 1). Solubility in 40% PEG 400 dropped dramatically for LDN-193665 and -213828. LDN-193594 remained soluble at a concentration of 12 mg/ml. LDN-213842 and -213843 have better aqueous solubility (100 and 1000 μM, respectively) than LDN-213828, consistent with the calculated Log*P* values, although their PEG 400 solubility was lower than that of LDN-213828.

Pharmacokinetics of the diaminothiazoles was studied in the 3×Tg-AD mice. LDN-193594 was administered i.p., and its concentration was measured in plasma and brain samples at different times after injection (Fig. 2*A*). Data were fitted to a one-compartment model (see "Experimental Procedures"). The parameters obtained are indicated in Fig. 2*A, inset table*. LDN-193594 is rapidly absorbed and permeates the blood brain barrier, reaching C_{max} at 10 min, with 161 μM observed in plasma and 69 μM in brain. The average plasma brain ratio calculated is 0.34 ± 0.04. This concentration is ~2000-fold the calculated IC_{50} and 12-fold the EC_{50} observed. LDN-193594 clearance appears faster in the brain than in the plasma, with a calculated half-life of 0.71 h in the brain and 1.2 h in plasma.

We tested CDK5 activity *in vivo* after injection with LDN-193594 using the immunoprecipitation method previously described (16, 25). Young adult mice (1 month old CD1) were i.p.-injected with 120 mg/kg LDN-193594. After 15 min, mice were euthanized with CO_2, the brains removed, and cortex lysates homogenized and immunoprecipitated with CDK5 antibody or isotype immediately (Fig. 2*B*). [γ-^{32}P]ATP phosphotransfer to H1 peptide was tested by *in vitro* radioactivity kinase assay (Fig. 2, *C* and *D*). Data are reported as percentage of ^{32}P transfer to H1 in treated mice compared with vehicle mice. CDK5 activity in the mice treated with LDN-193594 was reduced 37% (Fig. 2*E*) ($n = 4$, $p = 0.064$).

LDN-213828 and LDN-213843 were i.v. administered. LDN-213828 permeates the blood brain barrier with an average brain plasma ratio of 0.25 ± 0.06. The C_{max} in the brain was 31 μM, detected 5 min after injection. LDN-213843 was undetectable in brain lysates. This result was partially predictable by theoretical analysis; as a general rule, compounds with a polar surface area of <90 Å^2 and a number of hydrogen bond donors of <3 (26) may have better blood brain barrier permeability; the polar surface area of LDN-213843 is 96 Å, and it has four hydrogen bond donors.

We concluded that LDN-193594, -193665, and -213828 were leads for assessing the effects of this diaminothiazole series *in vivo*. Because of structural similarities between LDN-193594 and -193665, we decided to assess LDN-193594, the most potent inhibitor *in vitro*, and LDN-213828, the most biostable inhibitor of our series. We assessed the toxicity of these *in vivo*. LDN-193594 was administered i.p. at 120, 60, and 30 mg/kg/day for 7 consecutive days. Two of the three mice treated with the maximum dose died after 3 days of treatment. The third mouse presented major body weight loss by day 5, surpassing the established end point of losing more than 15% of the original weight. Six mice treated with all other doses assayed, vehicle (40% PEG 400) or PBS, suffered no major weight loss, with a maximum weight loss averaging 6% (Fig. 2*F*). In addition, mice displayed no symptoms of pain or distress; they groomed and ate normally and appeared active. Four mice per group treated with 78 or 39 mg/kg/day LDN-213828 or vehicle (60% PEG 400), by similar methodology, displayed no evident signs of toxicity and experienced a maximum weight loss averaging 8%.

Treatment with Diaminothiazole Kinase Inhibitors Exerts Neuroprotective Effects in Vivo—Compounds LDN-193594 and -213828 were studied in two mouse models via various administration methods as summarized in Table 1. Neuronal protective effects were immunohistochemically evaluated by visualiz-

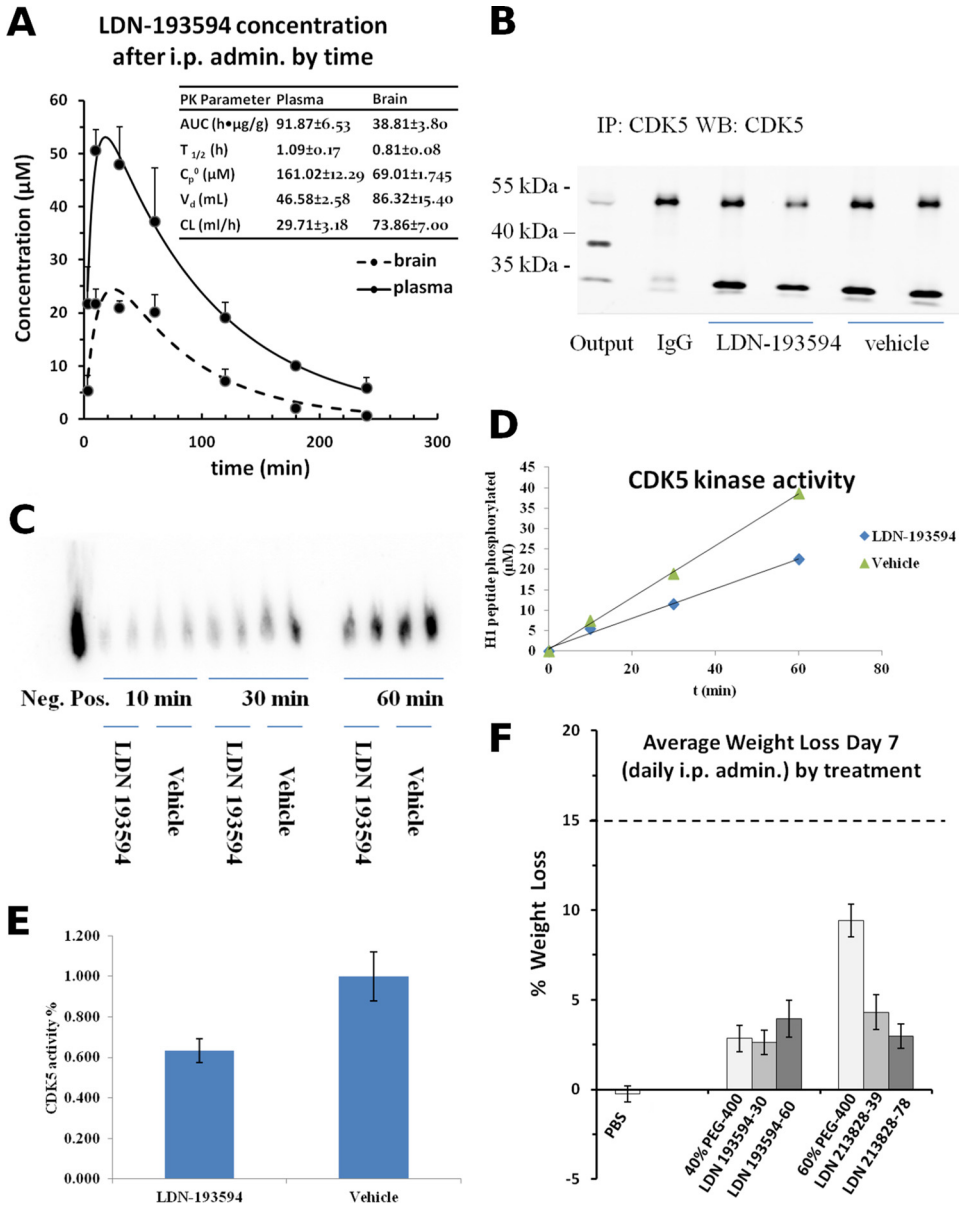

FIGURE 2. **Pharmacokinetics, *ex vivo* CDK5 inhibition, and toxicity of diaminothiazole kinase inhibitors.** *A,* concentration of LDN-193594 in plasma (*continuous line*) and brain (*dashed line*) was measured using HPLC/UV. Data are shown as concentration (µM) measured in mean ± S.E. Pharmacokinetics parameters obtained are reported in the *inset*. Average plasma brain ratio of 0.34 ± 0.04 was calculated from the brain and plasma concentration at each time point. *AUC,* area under the concentration-time curve; V_d, volume of distribution; $T_{1/2}$, elimination half-life derived from the quotient of 0.693 and the elimination rate constant; C_{max}, maximum concentration measured; *Cl,* clearance, derived from the equation $Cl = V_d \cdot 0.693/T_{1/2}$. *B–E, ex vivo* kinase assay confirmed that LDN-193594 reduces CDK5 kinase activity. *B,* CDK5 was immunoprecipitated from 1-month-old CD1 mice 15 min after i.p. injection of the drug candidate or the vehicle. CDK5 activity was immediately measured by *in vitro* radioactivity kinase assay. Representative Western blot image for CDK5 immunoprecipitation was probed with rabbit anti-CDK5 antibody. *C,* radioactivity of the phosphorylated H1 peptide as the CDK5 phosphorylation product was detected on p81 phosphocellulose paper at reaction times of 10, 30, and 60 min. The reaction with the recombinant CDK5/p25 was used as a positive control, and in the negative control the enzyme was replaced with the protein fraction using IgG immunoprecipitation. *D,* representative data show the linear rate of product formation, presented by concentration of the phosphorylated H1 peptide (µM) over time (min). *E, bar graph* demonstrates that the reaction rate from mice that had been treated with a single injection of 120 mg/kg LDN-193594 is 37% reduced compared with the mice treated with vehicle alone. Data are presented as mean ± S.E. $n = 4$. $p = 0.064$. *F,* daily i.p. administration of diaminothiazoles for 1 week did not cause major weight loss. Average body weight loss at day 7 is shown as mean ± S.E. Mice treated with 120 mg/kg/day were removed from the assay at or before day 5 due to 15% body weight loss. Mice treated with all other doses survived the experiment.

ing NFT formation with the PHF-1 antibody, and neuronal survival or DNA damage was evaluated using antibodies to NeuN or γH2AX. Quantification of the signal was performed in the CA1 area of hippocampus. Tau phosphorylation was assessed by Western blotting with the PHF-1 antibody.

In vivo efficacy of the diaminothiazole inhibitors in PHF-1$^+$ neurons was assayed in a CK-p25 mouse model 6 weeks after induction. In these mice, the induction of p25-eGFP expression in the brain causes CDK5 activation. The neurotoxicity associated with p25 overexpression is progressive. Two weeks after p25-eGFP induction, cell death and learning and memory impairment were not yet present, and virtually all neurons in the pyramidal layer expressed the transgene that fills the cytoplasm, and cells present an extensive dendritic arborization similar to the morphology of healthy control CA1 pyramidal neurons (Fig. 3*A*). After 6 weeks, p25-eGFP is mostly limited to

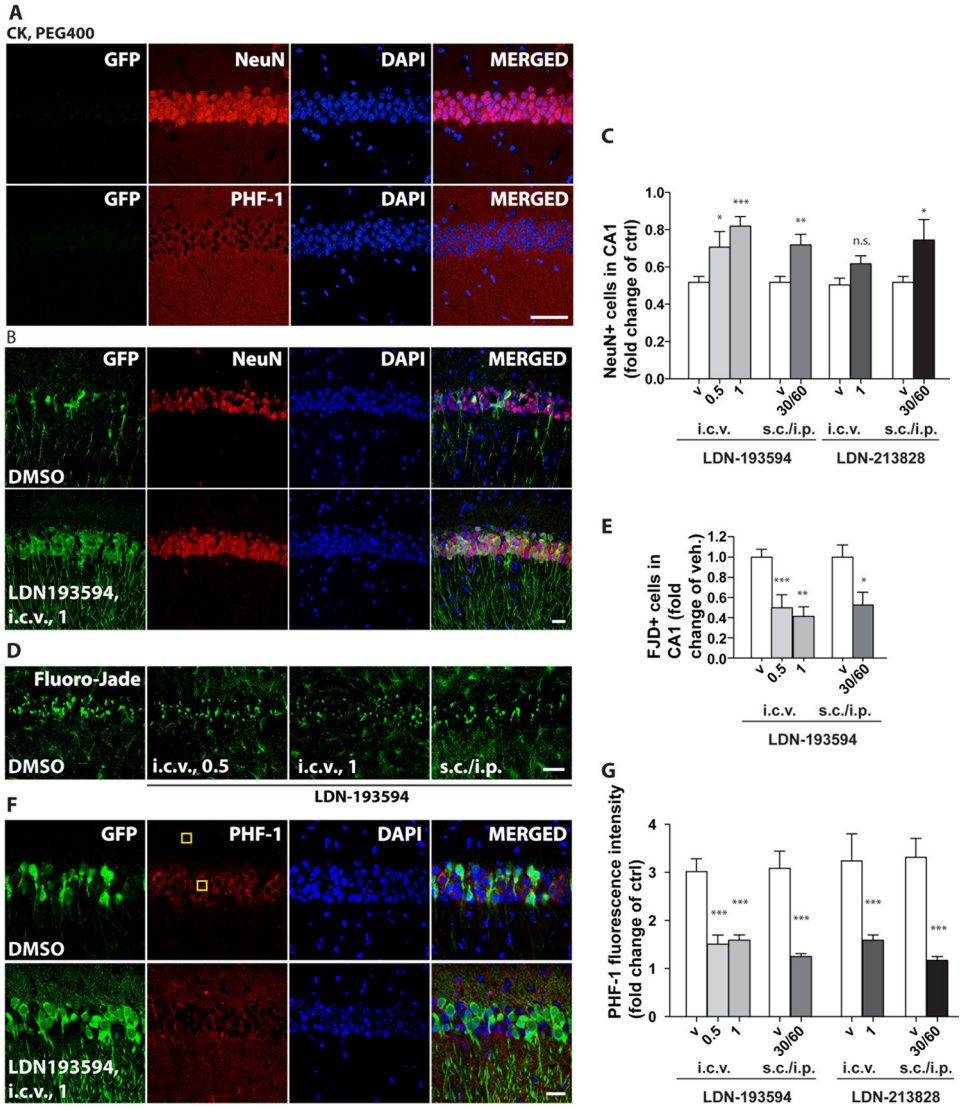

FIGURE 3. **Neuroprotective effect in diaminothiazole-treated CK-p25 mice.** Mice were sacrificed by intracardiac perfusion. Brains were collected, post-fixed overnight, and sliced at a 40-μm width. Brain slices were stained with anti-NeuN or PHF-1 followed by anti-mouse IgG1-Alexa 594 or stained with Fluoro-Jade. Nuclei were counter-stained using DAPI. High resolution $\times$40 confocal images displaying CA1 pyramidal layer of the hippocampal region at Bregma -1.90 mm were acquired ($n \geq 3$), *bar*, 40 μm. *A*, representative images display NeuN and PHF-1 immunoreactivity in the uninduced CK-p25 mice. *B*, increased number of $NeuN^+$ cells are observed in diaminothiazole-treated CK-p25. Mice were i.c.v.-treated for 6 weeks with LDN-193594 at 1 mg/kg/day or vehicle (50% DMSO) using subcutaneously implanted Alzet pumps (experiment 1). *C*, *histogram* summarizes the neuroprotective effect observed after diaminothiazole treatment in experiments 1–5 as compared with vehicle (*v*). $NeuN^+$ cells were counted using ImageJ cell counter plugin, and the number of $NeuN^+$ cells per CA1 region was calculated (mean $\pm$ S.E.). *D*, representative images show a decreased number of $Fluoro\text{-}Jade^+$ cells are observed in LDN-193594-treated CK-p25 mice via i.c.v. at the dose of 0.5 or 1 mg/kg or via s.c./i.p. at the dose of 30/60 mg/kg (experiments 1, 2, and 4). *E*, *histogram* summarizes the neuroprotective effect observed based on the Fluoro-Jade staining. *F*, perinuclear mislocalized PHF-1 immunoreactivity is reduced by diaminothiazole treatment (experiment 1). *G*, *histogram* summarizes the average fluorescence intensity of PHF-1 in experiments 1–5, quantified in two regions of the CA1 pyramidal layer, a perinuclear and a neuritic region, as indicated by *yellow squares* presented in *F*. The fluorescence ratio of perinuclear to neuritic region was calculated, and values were normalized to that of vehicle. Normalized data are presented as mean $\pm$ S.E. Where applicable, statistical significance is indicated with *n.s.*, not significant; *, $p < 0.05$; **, $p < 0.01$; ***, $p < 0.001$.

a few remaining pyramidal cell bodies and does not extend into the dendritic region, most likely reflecting cellular atrophy associated with the neurotoxicity (Fig. 3*B*). Extensive neurotoxicity occurring in the CA1 region of the hippocampus is associated with deficits in learning and memory (9, 20). Mice that were treated with LDN-193594 i.c.v. for 6 weeks after p25 induction showed a cytoplasmic and dendritic pattern of p25-eGFP distribution similar to that at an earlier time after induction, including a higher number of cells expressing the transgene, implicating a reduction in the cellular atrophy associated with p25 overexpression.

NeuN staining was used to assess the extent of neuronal loss in these mice. The average number of CA1 neurons was reduced from 2100 $\pm$ 20.00 $NeuN^+$ cells/mm^2 in control CK mice (representative image shown in Fig. 3*A*) to 1200 $\pm$ 61.24 in CK-p25 mice, 6 weeks after p25 induction (Fig. 3*A*). $NeuN^+$ density recovered to 1692 $\pm$ 109.6 for mice that received LDN-193594 i.c.v. and to 1764 $\pm$ 100.49 following s.c./i.p. treatment. This improvement corresponds to $\sim$ 40% recovery in both cases (Fig. 3, *B* and *C*). A neuroprotective effect was also observed in mice treated with LDN-213828 i.c.v. but did not achieve statistical significance; however,

systemic delivery of this compound gave a 48% recovery ($p < 0.05$).

Fluoro-Jade stain is a fluorochrome derived from fluorescein and is commonly used to stain degenerating neurons. This method was validated in models of cell death such as kainic acid (27), 1-methyl-4-phenyl-1,2,3,6-tetrahydropyridine (28), or multivalent metals (29) *in vivo* and showed similar results as quantification of cell death using conventional hematoxylin and eosin, Nissl, or de Olmos' cupric-staining methodologies (30). Typically, Fluoro-Jade-positive neurons also present a condensation of the chromatin, a disruption of the plasma membrane, and nuclear membrane integrity. The neuroprotective effect of LDN-193594 was confirmed as the number of degenerating neurons was reduced 60% in the treatment with LDN-193594 at 1 mg/kg dose, 50% at 0.5 mg/kg dose by i.c.v., and 50% at 30/60 mg/kg dose by s.c./i.p. (Fig. 3, *D* and *E*).

Neuronal toxicity associated with p25-eGFP expression was supported by the observation of intense perinuclear PHF-1 signal in CA1 pyramidal neurons in untreated mice following 6 weeks of p25 induction (Fig. 3*F*), and it was significantly reduced in mice treated i.c.v. with LDN-193594. The treated PHF-1 staining pattern was similar to that of uninduced CK-p25 mice (Fig. 3*A*). To quantify those changes, we measured the fluorescence intensity of PHF-1 and calculated the signal ratio between background and the perinuclear area of CA1 (indicated by the *yellow squares* in Fig. 3*F*), and we normalized it to the ratio in the vehicle (DMSO)-treated CK-p25 mice. The ratio was found to increase after p25 induction reflecting the accumulation of the PHF-1 signal around the cell body, whereas treatment with LDN-193594 by either i.c.v. or s.c./i.p. administration significantly reduced this ratio and the perinuclear aggregation of PHF-1. LDN-213828 also proved effective when administered s.c/i.p. for the last 3 weeks, in a similar manner (Fig. 3*G*).

3×Tg-AD mice (23 months old) were also treated with LDN-193594 by daily i.p. administration for 1 week. Immunohistological presence of PHF-1$^+$ neurons in the hippocampi was evaluated. This AD mouse model harbors mutations that cause the presence of both β-amyloid plaques and Tau NFTs in an age-related manner. Previously, transmission electron microscopy detected straight Tau filaments, immunoreactive to the phosphorylated Tau antibodies, Alz50 and AT8 at 23 months of age, but not at 2 or 9 months (31). By analyzing a series of coronal slices spanning most of the hippocampus rostrocaudally, we observed PHF-1$^+$ cells mainly in the CA1 area, with occasional detection in CA2 and dentate gyrus. These PHF-1$^+$ neurons appear to predominate in the dorsocaudal CA1, with a peak of detection around Bregma −1.5-mm slices. Mice treated i.p. with vehicle alone (40% PEG 400) presented an extensive amount of PHF-1$^+$ neurons in the CA1 pyramidal layer in the posterior hippocampus; mice treated i.p. with LDN-193594 (30 and 60 mg/kg/day) show few detectable PHF-1$^+$ neurons (Fig. 4*A*). A similar reduction occurred in mice that were treated with LDN-213828 compared with vehicle (60% PEG 400) in PHF-1$^+$ neurons (Fig. 4*A*).

Co-staining with Hoechst 33342 allowed us to calculate the density of nuclei in this area as ~2000 nuclei/mm^2. The number of nuclei quantified in mice with different treatments did not change (Fig. 4*B*). The number of PHF-1$^+$ CA1 neurons per 100 nuclei was quantified to 11.6 ± 0.25 in the vehicle-treated mice. LDN-193594 i.p. treatment significantly reduced this number to 0.12 ± 0.02 (60 mg/kg/day). PHF-1$^+$ neurons were undetectable in mice treated intraperitoneally with 39 mg/kg/day LDN-213828 and 4.5 ± 0.60% PHF-1$^+$ with a dose of 78 mg/kg/day (Fig. 4*C*). However, when LDN-193594 was administered via s.c. injection, the reduction in the number of PHF-1$^+$ neurons in the hippocampus was not significant (Table 1).

To assess the vulnerability of the neurons in the 3×Tg-AD mouse model, we aimed to evaluate the extent of DNA double strand breakage using a phospho-γH2AX antibody (32). Immunohistological co-labeling of 23-month-old 3×Tg-AD mice with PHF-1 and γH2AX showed detectable γH2AX foci present in CA1 neurons that also labeled with PHF-1$^+$. Although 3×Tg-AD mice treated with vehicle (40–60% PEG 400) presented a large amount of PHF-1$^+$ cells as well as γH2AX$^+$ cells (Fig. 4*D*), mice treated intraperitoneally with either LDN-193594 or LDN-213828 for a week showed a major reduction in cells with γH2AX foci (Fig. 4*E*). Quantification of the number of γH2AX$^+$ neurons in the CA1 region showed that 8.26 ± 0.70 γH2AX$^+$ cells per 100 nuclei were found in the CA1 region of the hippocampus. One week of i.p. treatment with LDN-193594 led to a 10-fold reduction (60 mg/kg/day) ($p < 0.01$), and treatment with LDN-213828 led to a 4-fold reduction (78 mg/kg/day) ($p < 0.05$). γH2AX$^+$ and PHF-1$^+$ cells were both undetectable when mice were treated with LDN-213828 at 39 mg/kg/day.

High resolution confocal micrographs with *Z*-stack three-dimensional reconstruction of double-labeled PHF-1/γH2AX slices showed that γH2AX is present in the perinuclear cytoplasm of PHF-1$^+$ cells in the hippocampus, instead of the expected nuclear compartment. The probability that a given γH2AX$^+$ cell was also stained with PHF-1 was equal to 0.97 ± 2.1. Therefore, most γH2AX$^+$ cells were also PHF-1$^+$ cells. The probability of co-localization did not change after treatment with diaminothiazoles which reduced both markers. This finding strongly suggests a link between NFT-bearing neurons and γH2AX DNA damage and is consistent with evidence from AD brains that show double-stranded breaks are more prevalent than in normal human aging brains (33). To our knowledge, abnormal cytosolic accumulation of γH2AX has not been previously described in the 3×Tg-AD model.

Diaminothiazole Kinase Inhibitors Reduce Tau Phosphorylation—To investigate the effect of the treatment on Tau phosphorylation in these mouse models, PHF-1 antibody was used. This antibody recognizes Tau phosphorylated at Ser-396 and Ser-404 (34). The PHF-1 immunoreactive signal, virtually undetectable in CK control mice (data not shown), has a very strong signal in the CK-p25 mice. Treatment of these mice with LDN-193594 and -213828 via i.c.v. for 6 weeks reduced the intensity of the PHF-1 immunoreactive band to nearly nondetectable levels (Fig. 5, *A* and *B*). A similar reduction was observed in s.c./i.p.-administered LDN-193594 and LDN-213828. To determine whether the observed reduction of NFTs (Fig. 4*A*) found in treated 3×Tg-AD mice correlated with the phosphorylation of Tau, we analyzed protein lysates of brains from 3×Tg-AD mice by Western blotting. In this model, a Tau band of ~65 kDa was enriched by fractionating Tau with Sarko-

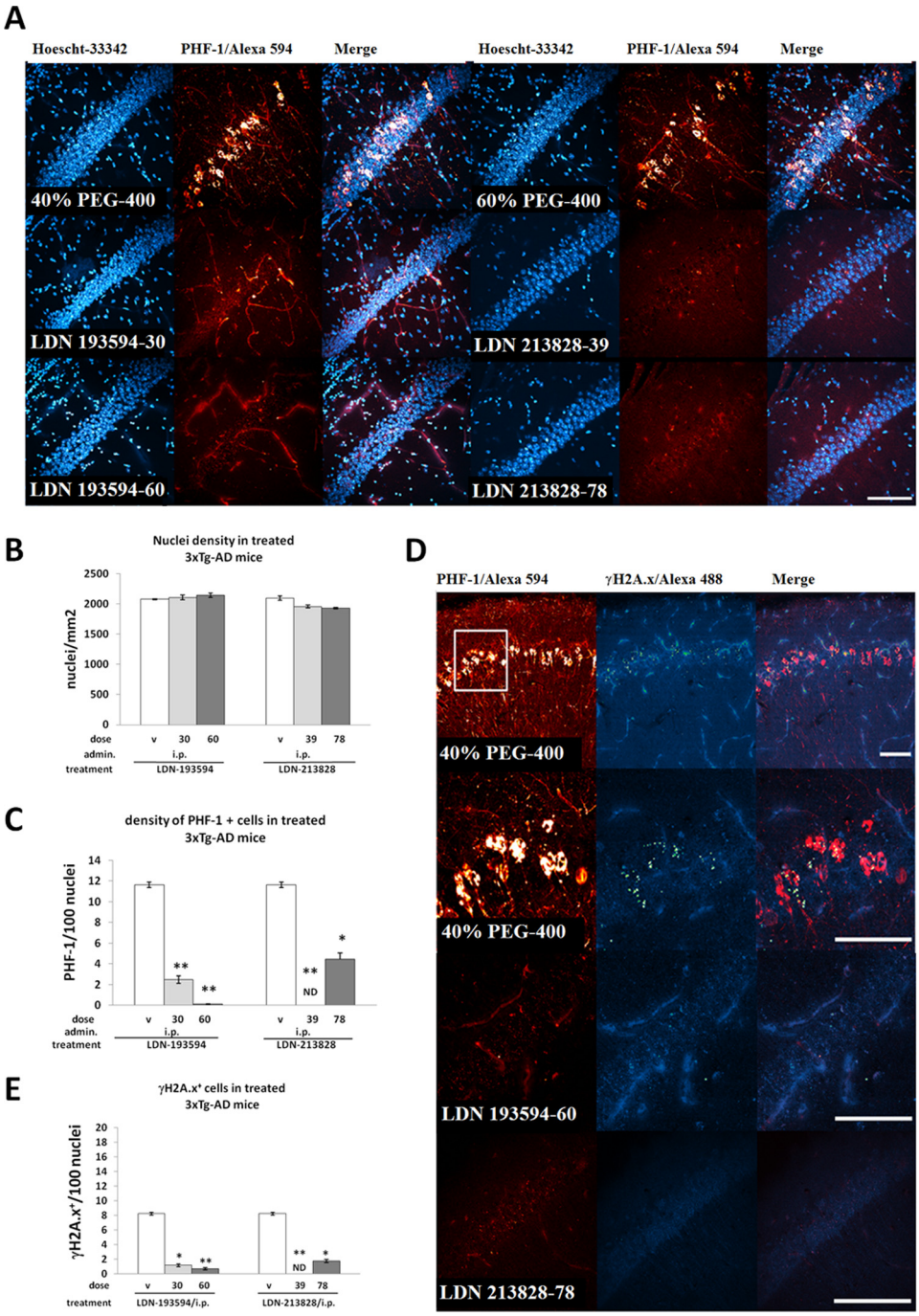

FIGURE 4. **Diaminothiazole treatment reduces PHF-1$^+$ and γH2AX$^+$ CA1 neurons in 3×Tg-AD mouse model.** *A*, PHF-1$^+$ immunoreactive cells indicative of NFTs in 3×Tg-AD mice were cleared by administration of diaminothiazoles. Aged 3×Tg-AD mice (23 months) were administered i.p. with vehicle (40–60% PEG 400) or either kinase inhibitor LDN-193594 (30 and 60 mg/kg/day) or LDN-213828 (39 and 78 mg/kg/day) for 1 week (experiments 6–9). Mice were sacrificed by intracardiac perfusion, and brains were post-fixed in 4% paraformaldehyde for an additional week. Coronal brain slices 50 μm thick were immunostained with mouse PHF-1 antibody and detected with anti-mouse IgG1 Alexa 594. Hoechst 33342 was used to stain cell nuclei. *Z*-stack confocal micrographs with 15 planes 1 μm each, spanning the CA1 pyramidal layer in at least four brain sections per mouse, were obtained at ×40 magnification and high resolution. Representative images are shown, displaying maximum *Z*-stack projections on Bregma −2.18 mm for mice with different treatments. *Bar*, 50 μm. *B*, CA1 pyramidal layer cell body density remains constant in vehicle (*v*) and diaminothiazole-treated 3×Tg-AD mice. Nuclei specifically located in the CA1 pyramidal layer were counted using ImageJ cells counter plugin in at least four sections per mouse. CA1 area was measured from the images, and nuclei density was calculated as nuclei/mm^2. Data are reported as mean ± S.E. *C*, PHF-1$^+$ immunoreactive cells were counted per image as indicated above, and a number of PHF-1$^+$ immunoreactive neurons in CA1 pyramidal layer for every 100 nuclei were calculated. Data are presented as mean ± S.E. *D*, reduction of Ser(P) histone γH2AX$^+$ cells associated with PHF-1$^+$ cells in CA1 pyramidal layer of treated 3×Tg-AD mice. The same tissue as indicated in *A* was stained with γH2AX. Representative maximum *Z*-stack projections on Bregma −1.00 mm are shown; *bar*, 50 μm. *E*, cells displaying foci of γH2AX and the nuclei in the CA1 pyramidal region were counted, and CA1 area was measured. Percentage of γH2AX$^+$ cells per nuclei was calculated and presented as mean ± S.E. Where applicable, statistical significance is indicated: *, $p < 0.05$, and **, $p < 0.01$. *ND* stands for not detected.

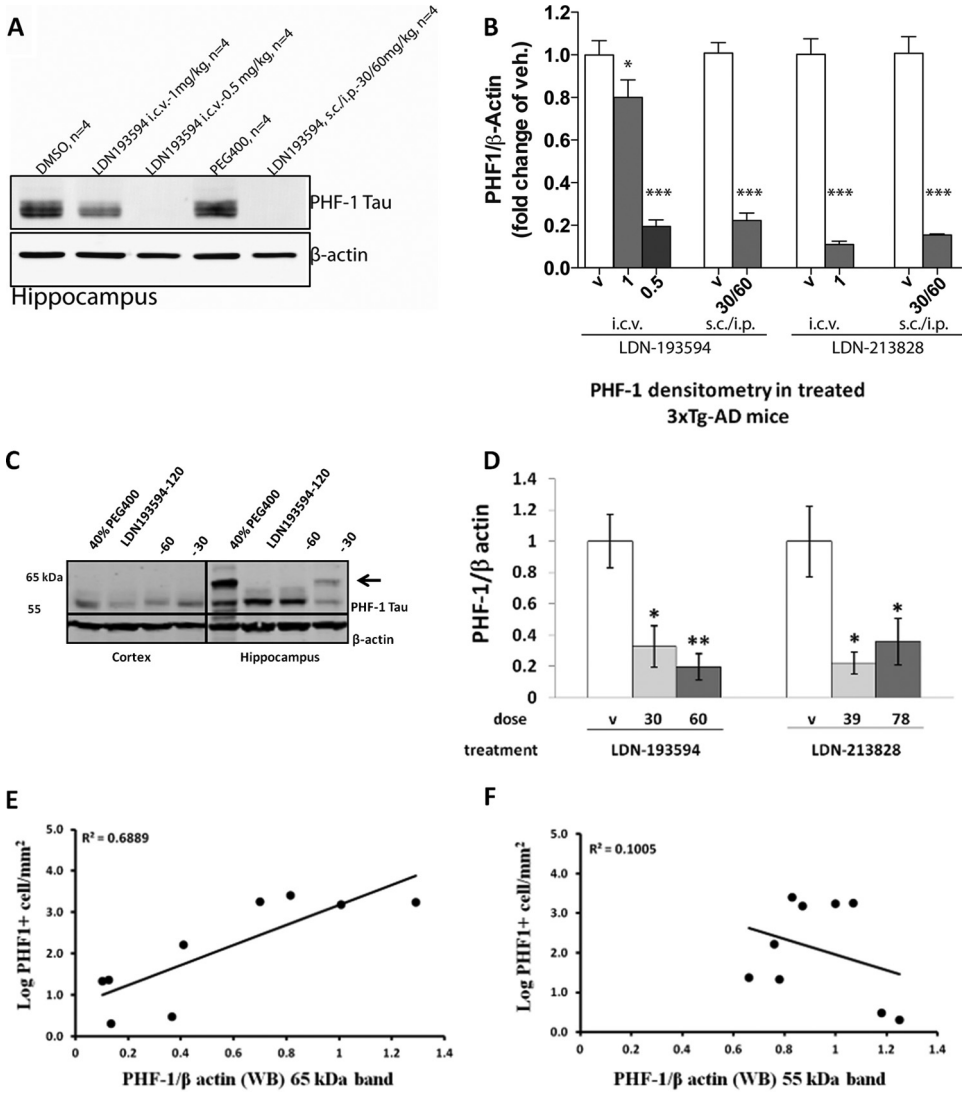

FIGURE 5. **Tau phosphorylation is reduced by kinase inhibitor diaminothiazole series *in vivo*.** *A* and *B*, phosphorylated Tau at 55 kDa detected by PHF-1 is reduced by diaminothiazole treatment in CK-p25 mice. *A*, representative images of the reduction in PHF-1 signal following treatment with LDN-193594 compared with the vehicle-treated mice (experiments 1, 2, and 4). Western blots of CK-p25 mice did not reveal a PHF-1 65-kDa band. *B*, ratio of PHF-1 to β-actin densitometry was calculated and normalized to vehicle (*v*). Normalized values are reported as mean ± S.E. $n \geq 3$. *C* and *D*, phosphorylated Tau at 65 kDa detected by PHF-1 was specifically reduced by diaminothiazole treatment in 3×Tg-AD mice. *C*, representative images showing reduction of PHF-1 signal following treatment with LDN-193594 compared with the vehicle-treated mice. Cortex (*left*) and hippocampus (*right*) are shown. The *arrow* indicates the 65-kDa phospho-Tau band reduced with treatment. *D*, ratio of PHF-1 to β-actin densitometry was calculated for the 65-kDa band in experiments 6–9, and normalized to vehicle. Normalized values are reported as mean ± S.E. $n \geq 4$. *E* and *F*, correlation of PHF-1$^+$ cell numbers with densitometry of 65 kDa (*E*) and 55 kDa (*F*) PHF-1 Tau bands by Western blotting. Statistical significance is indicated: *, $p < 0.05$, and **, $p < 0.01$.

syl and is likely to be comparable with the A68-hyperphosphorylated Tau band from human AD patients (35). Similar bands have been reported in JNPL3 mice containing the same human Tau mutation (36). After treatment with the vehicle or LDN-193594, the cortex and hippocampal lysates were analyzed (Fig. 5, *C* and *D*), and the 65-kDa Tau band was mainly observed in the hippocampus and strongly reduced in a dose-dependent manner by LDN-193594 treatment (Fig. 5*C*). The intensity of the 65-kDa band appeared strongly correlated with the numbers of PHF-1$^+$ neurons (Fig. 4*A*), $R^2 = 0.69$ (Fig. 5*E*). Other immunoreactive Tau bands with a lower apparent molecular weight did not show this correlation (Fig. 5*F*). The total Tau level, immunoblotted by antibody Tau-5, was not changed with LDN-193594 treatments compared with vehicle control (data not shown). We verified the reduction in the 65-kDa PHF-1 Tau band with LDN-193594 administered intraperitoneally at 30 and 60 mg/kg/day and with LDN-213828 administered intraperitoneally at 39 and 78 mg/kg/day (Fig. 5*D*).

Quantitative MS Confirms That Diaminothiazole Decreases Sarkosyl-insoluble PHF-Tau Levels as Well as Its Phosphorylation State—Protein samples were prepared from 23-month-old 3×Tg-AD mice treated with vehicle only (40% PEG 400) or LDN-193594 (60 mg/kg/day). Protein lysates from hippocampi were Sarkosyl-extracted to enrich for PHF-Tau. The Sarkosyl-insoluble pellet was separated via SDS-PAGE and probed with PHF-1 antibody to confirm enrichment of the PHF-Tau at 65 kDa. As described above, the PHF-Tau was strongly enriched in the vehicle-treated mice hippocampi. However, this band was not detected in the Sarkosyl fraction of the LDN-193594-treated mice (Fig. 6*A*).

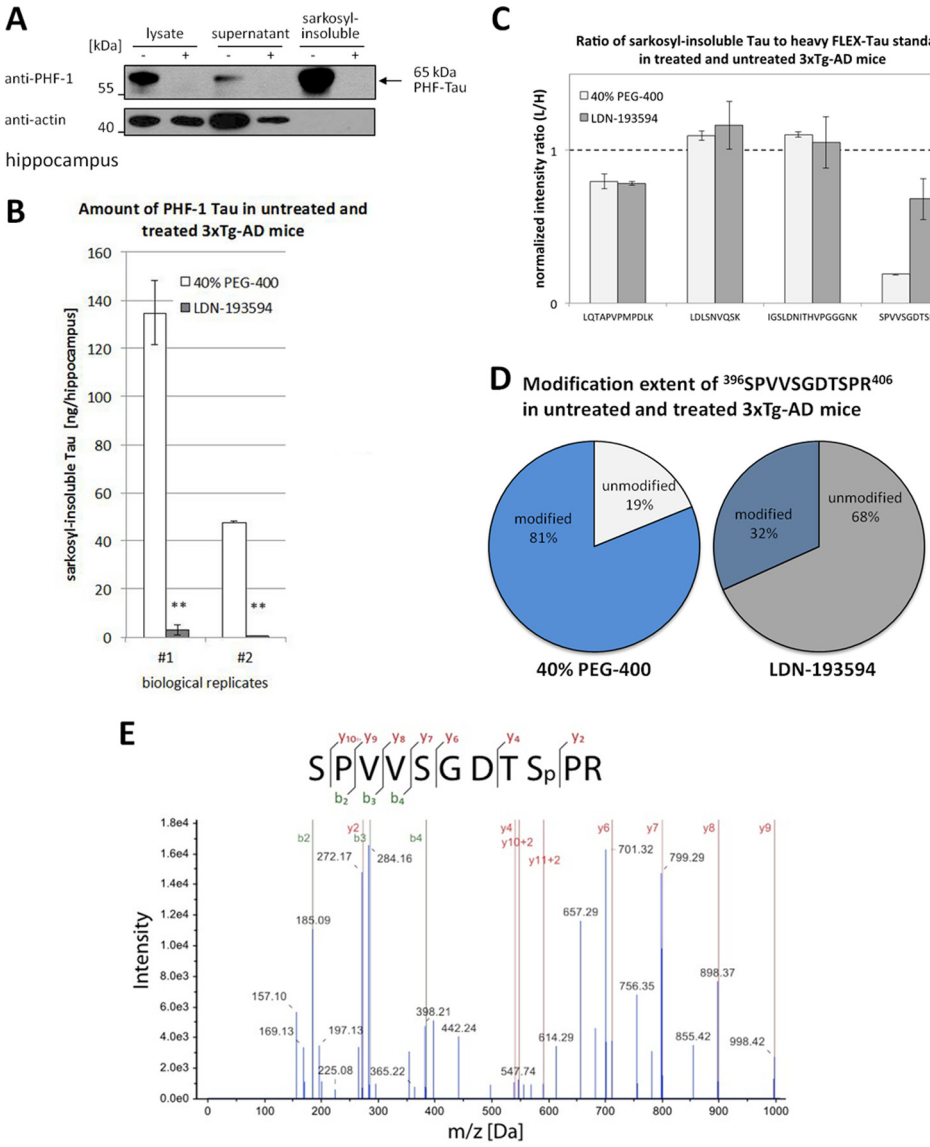

FIGURE 6. **Mass spectrometry of hippocampal protein lysate from 3×Tg-AD mice treated with either vehicle or LDN 193594.** *A,* hippocampi from 23-month-old 3×Tg-AD mice with either LDN-193594 (60 mg/kg/day) or vehicle alone by i.p. delivery were used to prepare a Sarkosyl-insoluble protein fraction. This Sarkosyl-insoluble fraction was separated by SDS-PAGE and probed with PHF-1 antibody. The immunoblot shows a clear enrichment for a 65-kDa phospho-Tau band in the Sarkosyl-insoluble fraction in the vehicle-only treated mouse, whereas the LDN-194594-treated mouse does not show a signal for this 65-kDa phospho-Tau protein. *B,* corresponding 65-kDa areas were excised from a Coomassie-stained gel and trypsinized from the LDN-193594 and vehicle-treated samples and quantified using our FLEX-Tau^{H} method using a scheduled multiple reaction monitoring assay. Absolute protein amounts were determined for the total Sarkosyl-insoluble PHF-Tau. Two independent biological replicates with three technical repeats each are shown. In both biological repeats, the amount of Tau in the PHF-1-positive fraction was significantly decreased in the LDN-193594-treated compared with vehicle condition. Data are presented as mean ± S.E. Statistical significance is indicated: **, $p < 0.01$. *C,* for this analysis, three representative peptides present in similar ratios and unchanged between vehicle- and LDN-193594-treated samples were used to normalize comparisons between samples. Light to heavy ratios of normalized intensity values for these three peptides as well as the tryptic peptide ^{396}SPVVSGDTSPR^{406} are shown ($n = 2$). Normalized data are presented as mean ± S.E. *D,* using the FLEXIQuant approach, the extent of modification of the peptide ^{396}SPVVSGDTSPR^{406} was calculated for vehicle-treated (40% PEG 400) and LDN-193594-treated 3×Tg-AD mice. The vehicle-treated sample exhibited 81% modification of the SPVVSGDTSPR peptide, whereas the LDN-193594-treated sample was 32%. Thus, LDN-193594-treated samples displayed a significantly decreased amount of PHF-1-positive insoluble Tau and a decreased extent of insoluble Tau modification. *E,* Sarkosyl-insoluble Tau of 3×Tg-AD mice samples treated with vehicle only was subjected to LC/MS/MS analysis on a Q Exactive tandem mass spectrometer. The MS/MS spectrum of the phosphopeptide ^{396}SPVVSGDTS$_p$PR^{406} is depicted. The y-series fragments support a mono-phosphorylation at either Thr-403 or Ser-404 (Ser-404 depicted exemplarily).

The absolute amount of Sarkosyl-insoluble Tau in the peptide mix was determined by analyzing L/H ratios of the quantified FLEX-Tau^{H} peptides to corresponding endogenous peptides, ^{243}LQTAPVPMPDLK^{254}, ^{282}LDLSNVQSK^{290}, and ^{354}IGSLDNITHVPGGGNK^{369}, which were unchanged between vehicle and LDN-193594-treated samples and were detected with high signal intensities in all technical and biological replicates. In two independent experiments, mice treated with LDN-193594 (3 and 0.4 ng/hippocampus) showed a reduction to ~1.5% in total Sarkosyl-insoluble PHF-Tau compared with vehicle-treated mice (135 and 48 ng/hippocampus (Fig. 6*B*).

Current models of the Tau phosphorylation pattern associated with AD point to two CDK5 phosphorylation sites, namely Ser-235 and Ser-404 (34). The extent of CDK5 activity on Tau could be measured by monitoring these sites. Tryptic peptides containing these sites were analyzed to determine their suit-

ability for quantitative measurements. The Ser-235 site is located on peptide ^{235}SPSSAK^{240} in a tryptic digest. This peptide was not detectable even with multiple reaction monitoring methods, and therefore quantification of this modification site was not possible. We therefore focused on the tryptic peptide containing the phosphorylation site at Ser-404 (^{396}SPVVSGDTpSPR^{406}), which coincides with a recognition site of the PHF-1 antibody. Peptide intensities were normalized for different amounts of Tau in each sample using the above-mentioned unmodified peptides. In Sarkosyl-insoluble Tau samples of vehicle-treated 3×Tg-AD mice, 19% of this peptide is unmodified and 81% is modified, whereas after treatment with LDN-193594, 68% is unmodified and 32% modified (Fig. 6*C*). Thus, the modification of this tryptic peptide in Sarkosyl-insoluble PHF-Tau of 3×Tg-AD mice decreased by 60% upon treatment with LDN-193594.

The FLEXIQuant approach provides information about the extent of modifications based on the reduction of the respective unmodified peptides; however, it does not provide information about the type of modification and the amino acid-specific localization of the modification. As immunoreactivity with PHF-1 antibody (34) suggests the occurrence of Tau phosphorylation on Ser-396 and Ser-404 in these samples, we performed a phosphorylation analysis by LC/MS/MS of Sarkosyl-insoluble Tau from 3×Tg-AD mouse hippocampi treated with vehicle only, targeting all possible phosphorylation sites using an inclusion list of *m/z* values corresponding to singly and doubly phosphorylated tryptic peptides. In these samples, we found spectral evidence for a single phosphorylation on the ^{396}SPVVSGDTSPR^{406} peptide at either Thr-403 or Ser-404 (Fig. 6*D*). Interestingly, diphosphorylation of the Tau peptide that would be predicted to occur at Ser-396 and Ser-404 was not identified. The concentration of this species may have been below the detection limit of the instrument, due to the low amount of Sarkosyl-insoluble Tau in the samples. However, it is likely that the diphosphorylated form of ^{396}SPVVSGDTSPR^{406} was less abundant than the monophosphorylated forms.

Diaminothiazole Kinase Inhibitor Restores the Learning and Memory Abilities—Finally, we investigated the effect of the LDN-193594 treatment on the learning and memory deficits in the CK-p25 mice. In this model, the neuronal loss following 6 weeks of p25 overexpression is associated with a deficit in hippocampus-dependent memory in the fear-conditioning task (20). To test the effect of the LDN-193594 treatment on this learning deficit, CK-p25 mice or CK-only control littermates were separated into two groups and treated either with LDN-193594 or vehicle. Alzet pumps delivered a 2-week subcutaneous infusion during weeks 4 and 5 of p25 induction, followed by i.p. injection during the 6th week. At that time, the hippocampus-dependent cognitive ability of those mice was tested in contextual fear conditioning, with a training phase followed by a testing phase 24 h later. Freezing results from the CK control mice receiving either vehicle or LDN-193594 showed similar freezing behaviors in this task with no statistical differences between the two groups. However, CK-p25 mice treated with vehicle showed a 48% decrease in their learning abilities in contextual fear conditioning compared with control CK mice. This deficit in the LDN-193594-treated mice was rescued to the levels of control CK mice following LDN-193594 treatment as the learning abilities of those mice were no longer statistically significant from the control mice (Fig. 7, *A* and *B*). This result showed that the positive effect of the treatment on both neuronal survival and Tau phosphorylation also translated into a rescue of the learning abilities of the CK-p25 mice in this learning and memory task.

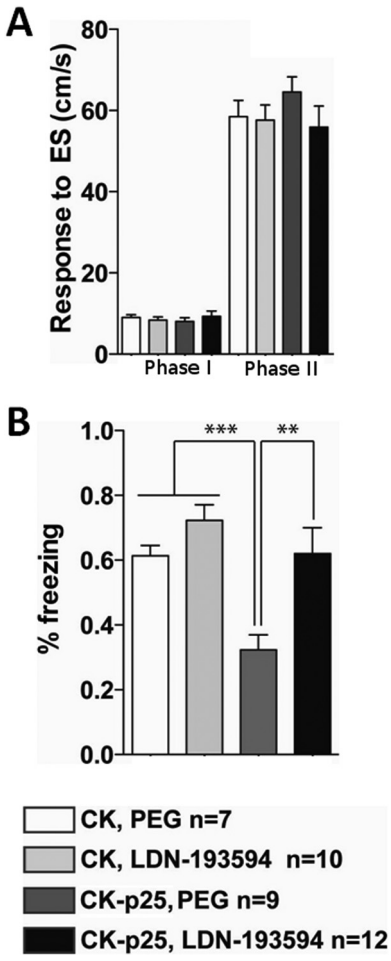

FIGURE 7. **LDN-193594 treatment recovers the learning and memory abilities of CK-p25 mice examined in contextual fear conditioning.** *A,* response to the external stimulus (*ES*) during phases one and two was measured and showed no difference between the four experimental groups. *B,* percentage freezing in CK-p25-induced mice are increased from 25% in vehicle-treated mice to 60% with LDN-193594 treatment, a level comparable with learning and memory abilities of the control CK vehicle-treated mice. Statistical significance is indicated: **, $p < 0.01$; ***, $p < 0.001$.

DISCUSSION

A small molecule in the chemical class of diaminothiazoles can inhibit Tau phosphorylation and exert neuroprotective effects in two distinct, well known AD mouse models as follows: 3×Tg-AD (17) mice that contain both Aβ amyloid and neurofibrillary tangles, and CK-p25 (9) mice with up-regulated CDK5 activity and neurofibrillary tangles. The *in vivo* neuroprotective effect is mediated in part by inhibition of Tau phosphorylation at sites identified by mass spectrometry of the insoluble Tau in the 3×Tg-AD model. Furthermore, in the CK-p25 model, treatment also resulted in a recovery of memory in a fear conditioning assay. The lead compound in this study, LDN-193594,

emerged from HTS and medicinal chemistry as a potent inhibitor of both CDK5/p25 and GSK3β (19). LDN-193594 has favorable chemical properties with a *c*Log*P* of 3.1, a polar surface area of 83 Å^2, and aqueous solubility of >20 μM. It passes the blood brain barrier and was observed at a concentration of 161 μM in plasma and 69 μM in the brain with an average plasma brain ratio of 0.34 $\pm$ 0.04. Formulation with PEG 400 greatly improved the solubility of the diaminothiazole compounds (Fig. 1). LDN-193594 can be solubilized in 40% DMSO, 22% 2-hydroxypropyl-β-cyclodextrin in 0.9% saline up to 50 mg/ml, but 2-hydroxypropyl-β-cyclodextrin can alter Tau and Aβ aggregation (37). With 40% PEG in water, 12 mg/ml solubility was reached, a concentration that allowed for a 120 mg/kg dose for i.p. injection in adult mice, which leads to inhibition of CDK5 kinase activity in mice observed in *ex vivo* kinase assay. The compound showed no sign of toxicity within our therapeutic dose range. Blocking the 6-position of the 3-pyridine (LDN-212853 and LDN-213828) resulted in an extension of the half-life (Fig. 1). However, a metabolite of LDN-193594 with a molecular weight of 490, which represents a 176 mass increase above the parent molecule was present in plasma, but not in the brain, indicating the possibility of a glucuronide reaction in plasma that modifies the compound *in vivo* through other metabolic pathways.

The drug effect on Tau pathology in 3×Tg-AD mice was observed by both Western blot and immunohistochemistry with PHF-1 antibody. PHF-1 antibody selectively recognizes phosphorylated Ser-396/Ser-404 of Tau (23, 34) and labels NFTs in tissue (31). Western blots from 3×Tg-AD brains showed that a 65-kDa PHF-1 immunoreactive band correlated with the number of hippocampal NFTs. The phosphorylation status of the Tau band is based on the observation that after treatment by phosphatase the band co-migrated with nonphosphorylated recombinant Tau (39). Quantitative mass spectrometry analysis confirmed this observation by showing that the amount of PHF-1-positive Tau in the LDN-193594-treated samples was reduced to ~1.5% of that observed in the vehicle-treated control samples. Furthermore, the residual 2% of Tau found in the Sarkosyl-insoluble fraction, which migrated at 65 kDa, showed a reduction in the extent of phosphorylation of a peptide containing a CDK5-dependent consensus site ^{396}SPVVSGDTSPR^{406}. The fact that the treatment with the CDK5/GSK3-β inhibitors used in this study reduced the phosphorylation of Tau as detected by Western blot, immunohistochemistry, and mass spectrometry provides strong evidence that the small molecular kinase inhibitor treatment could slow the progression of Tau pathology. 23-Month-old 3×Tg-AD mice have extensive PHF-1 immunoreactivity. Whether these immunoreactive inclusions represent neurofibrillary tangles or some other form of abnormally phosphorylated Tau is unknown. However, the relatively rapid clearance of the PHF-1 immunoreactivity with LDN-193594 treatment suggests that many of the inclusions in the 3×Tg-AD mice at 23 months of age have not aggregated into highly compact and resilient paired helical filaments but remained exchangeable with a more soluble Tau compartment (31).

Treatment with LDN-193594 in the CK-p25 mice dramatically affected the prominent neuronal cell loss that accompanies increased CDK5 activity (9). Using NeuN and Fluoro-Jade as markers, the neuronal loss at 6 weeks of p25 overexpression was rescued to the level seen in control mice. The fact that the inhibitor was able to block the accumulation of the fluorescent PHF-1 signal in the perinuclear area of CA1, while maintaining the expression pattern of p25-eGFP to a state of early induction where no cellular loss had yet occurred, argues for a neuroprotective effect of the drug (Fig. 3).

Treated mice also improved in a fear-conditioning task. At 6 weeks after induction, CK-p25 mice have accumulated hyperphosphorylated Tau with extensive neuronal cell loss and a severe diminution in memory as measured by two hippocampus-dependent tasks as follows: fear conditioning and the Morris water maze (20). When treated with LDN-193594, CD-p25 mice performed the fear conditioning task as well as the control mice. The recovery of memory function using this model was nonpharmacologically demonstrated by restoring memory in an inducible CDK5 conditional knock-out mouse (40).

The lead compound, LDN-193594, inhibits both GSK3β and CDK5 nearly equally when tested at the same ATP concentration. This property of dual kinase inhibition may be related to its efficacy in these studies. Many Tau residues that are typically found phosphorylated in insoluble Tau can be phosphorylated by CDK5 and GSK3β. There exists considerable overlap and cooperation between these two kinases (41). Like CDK5-overexpressing mice, GSK3β-overexpressing mice also display characteristics typical of AD such as hyperphosphorylation of Tau as well as learning and memory deficits (38, 42). Effective therapies for tauopathies such as frontotemporal dementia and the tauopathy associated with Alzheimer disease may require inhibition of both kinases.

Acknowledgment—We thank Peter Davies for the generous gift of PHF-1 antibody.

REFERENCES

1. Wischik, C., and Staff, R. (2009) Challenges in the conduct of disease-modifying trials in ad: Practical experience from a phase 2 trial of TAU-aggregation inhibitor therapy. *J. Nutr. Health Aging* **13,** 367–369
2. Chai, X., Wu, S., Murray, T. K., Kinley, R., Cella, C. V., Sims, H., Buckner, N., Hanmer, J., Davies, P., O'Neill, M. J., Hutton, M. L., and Citron, M. (2011) Passive immunization with anti-Tau antibodies in two transgenic models. *J. Biol. Chem.* **286,** 34457–34467
3. Schmechel, D. E., Gerard, G., Vatakis, N. G., Harper, L., Ross, J. S., Bari, M., Walling, D., Stedman, M., Winston, J. L., Morimoto, B., and Keith, J. R. (2008) P2-377: A phase 2, double-blind, placebo-controlled study to evaluate the safety, tolerability, and effect on cognitive function of AL-108 after 12 weeks of intranasal administration in subjects with mild cognitive impairment. *Alzheimers Dement.* (suppl), **4,** T483
4. Domínguez, J. M., Fuertes, A., Orozco, L., del Monte-Millán, M., Delgado, E., and Medina, M. (2012) Evidence for the irreversible inhibition of glycogen synthase kinase-3β by tideglusib. *J. Biol. Chem.* **287,** 893–904
5. Helal, C. J., Kang, Z., Lucas, J. C., Gant, T., Ahlijanian, M. K., Schachter, J. B., Richter, K. E., Cook, J. M., Menniti, F. S., Kelly, K., Mente, S., Pandit, J., and Hosea, N. (2009) Potent and cellularly active 4-aminoimidazole inhibitors of cyclin-dependent kinase 5/p25 for the treatment of Alzheimer's disease. *Bioorg. Med. Chem. Lett.* **19,** 5703–5707
6. Helal, C. J., Sanner, M. A., Cooper, C. B., Gant, T., Adam, M., Lucas, J. C., Kang, Z., Kupchinsky, S., Ahlijanian, M. K., Tate, B., Menniti, F. S., Kelly, K., and Peterson, M. (2004) Discovery and SAR of 2-aminothiazole inhibitors of cyclin-dependent kinase 5/p25 as a potential treatment for Alzhei-

mer's disease. *Bioorg. Med. Chem. Lett.* **14**, 5521–5525
7. Beaudette, K. N., Lew, J., and Wang, J. H. (1993) Substrate specificity characterization of a cdc2-like protein kinase purified from bovine brain. *J. Biol. Chem.* **268,** 20825–20830
8. Paudel, H. K., Lew, J., Ali, Z., and Wang, J. H. (1993) Brain proline-directed protein kinase phosphorylates tau on sites that are abnormally phosphorylated in tau associated with Alzheimer's paired helical filaments. *J. Biol. Chem.* **268,** 23512–23518
9. Cruz, J. C., Tseng, H.-C., Goldman, J. A., Shih, H., and Tsai, L.-H. (2003) Aberrant Cdk5 activation by p25 triggers pathological events leading to neurodegeneration and neurofibrillary tangles. *Neuron* **40,** 471–483
10. Noble, W., Olm, V., Takata, K., Casey, E., Mary, O., Meyerson, J., Gaynor, K., LaFrancois, J., Wang, L., Kondo, T., Davies, P., Burns, M., Veeranna, Nixon, R., Dickson, D., Matsuoka, Y., Ahlijanian, M., Lau, L. F., and Duff, K. (2003) Cdk5 is a key factor in tau aggregation and tangle formation *in vivo*. *Neuron* **38,** 555–565
11. Ishiguro, K. (1992) Tau protein kinase I converts normal Tau protein into A68-like component of paired helical filaments. *J. Biol. Chem.* **267,** 10897–10901
12. Lew, J. (1994) Neuronal cdc2-like kinase is a complex of cyclin-dependent kinase 5 and a novel brain-specific regulatory subunit. *Nature* **371,** 423–426
13. Tsai, L. H., Delalle, I., Caviness, V. S., Jr., Chae, T., and Harlow, E. (1994) p35 is a neural-specific regulatory subunit of cyclin-dependent kinase 5. *Nature* **371,** 419–423
14. Ishiguro, K. (1994) Identification of the 23-kDa subunit of Tau protein kinase II as a putative activator of CDK5 in bovine brain. *FEBS Lett.* **342,** 203–208
15. Sundaram, J. R., Poore, C. P., Sulaimee, N. H., Pareek, T., Asad, A. B., Rajkumar, R., Cheong, W. F., Wenk, M. R., Dawe, G. S., Chuang, K.-H., Pant, H. C., and Kesavapany, S. (2013) Specific inhibition of p25/Cdk5 activity by the Cdk5 inhibitory peptide reduces neurodegeneration *in vivo*. *J. Neurosci.* **33,** 334–343
16. Piedrahita, D., Hernández, I., López-Tobón, A., Fedorov, D., Obara, B., Manjunath, B. S., Boudreau, R. L., Davidson, B., Laferla, F., Gallego-Gómez, J. C., Kosik, K. S., and Cardona-Gómez, G. P. (2010) Silencing of CDK5 reduces neurofibrillary tangles in transgenic Alzheimer's mice. *J. Neurosci.* **30,** 13966–13976
17. Oddo, S., Caccamo, A., Shepherd, J. D., Murphy, M. P., Golde, T. E., Kayed, R., Metherate, R., Mattson, M. P., Akbari, Y., and LaFerla, F. M. (2003) Triple-transgenic model of Alzheimer's disease with plaques and tangles: intracellular Aβ and synaptic dysfunction. *Neuron* **39,** 409–421
18. Ahn, J. S., Radhakrishnan, M. L., Mapelli, M., Choi, S., Tidor, B., Cuny, G. D., Musacchio, A., Yeh, L. A., and Kosik, K. S. (2005) Defining Cdk5 ligand chemical space with small molecule inhibitors of Tau phosphorylation. *Chem. Biol.* **12,** 811–823
19. Laha, J. K., Zhang, X., Qiao, L., Liu, M., Chatterjee, S., Robinson, S., Kosik, K. S., and Cuny, G. D. (2011) Structure-activity relationship study of 2,4-diaminothiazoles as Cdk5/p25 kinase inhibitors. *Bioorg. Med. Chem. Lett.* **21,** 2098–2101
20. Fischer, A., Sananbenesi, F., Pang, P. T., Lu, B., and Tsai, L.-H. (2005) Opposing roles of transient and prolonged expression of p25 in synaptic plasticity and hippocampus-dependent memory. *Neuron* **48,** 825–838
21. Abramoff, M. D., Magelhaes, P. J., and Ram, S. J. (2004) Image processing with ImageJ. *Biophotonics Int.* **11,** 36–42
22. Kvilekval, K., Fedorov, D., Obara, B., Singh, A., and Manjunath, B. S. (0000) Bisque: A platform for bioimage analysis and management. *Bioinformatics* **26,** 544–552
23. Greenberg, S. G., and Davies, P. (1990) A preparation of Alzheimer paired helical filaments that displays distinct tau proteins by polyacrylamide gel electrophoresis. *Proc. Natl. Acad. Sci. U.S.A.* **87,** 5827–5831
24. Singh, S., Springer, M., Steen, J., Kirschner, M. W., and Steen, H. (2009) FLEXIQuant: a novel tool for the absolute quantification of proteins, and the simultaneous identification and quantification of potentially modified peptides. *J. Proteome Res.* **8,** 2201–2210
25. Selenica, M. L., Jensen, H. S., Larsen, A. K., Pedersen, M. L., Helboe, L., Leist, M., and Lotharius, J. (2007) Efficacy of small-molecule glycogen synthase kinase-3 inhibitors in the postnatal rat model of tau hyperphosphorylation. *Br. J. Pharmacol.* **152,** 959–979
26. Hitchcock, S. A., and Pennington, L. D. (2006) Structure-brain exposure relationships. *J. Med. Chem.* **49,** 7559–7583
27. Olney, J. W., Rhee, V., and Ho, O. L. (1974) Kainic acid: a powerful neurotoxic analogue of glutamate. *Brain Res.* **77,** 507–512
28. Heikkila, R. E., Hess, A., and Duvoisin, R. C. (1984) Dopaminergic neurotoxicity of 1-methyl-4-phenyl-1,2,5,6-tetrahydropyridine in mice. *Science* **224,** 1451–1453
29. Sloot, W. N., van der Sluijs-Gelling, A. J., and Gramsbergen, J. B. (1994) Selective lesions by manganese and extensive damage by iron after injection into rat striatum or hippocampus. *J. Neurochem.* **62,** 205–216
30. Schmued, L. C., Albertson, C., and Slikker, W., Jr. (1997) Fluoro-Jade: a novel fluorochrome for the sensitive and reliable histochemical localization of neuronal degeneration. *Brain Res.* **751,** 37–46
31. Oh, K.-J., Perez, S., Lagalwar, S., Vana, L., Binder, L., and Muffson, E. (2010) Staging of Alzheimer's pathology in triple transgenic mice: a light and electron microscopic analysis. *Int. J. Alzheimer Dis.* **2010,** 780102, 24 pp
32. Rogakou, E. P., Pilch, D. R., Orr, A. H., Ivanova, V. S., and Bonner, W. M. (1998) DNA double-stranded breaks induce histone H2AX phosphorylation on serine 139. *J. Biol. Chem.* **273,** 5858–5868
33. Keystone Symposium (2013) *New Frontiers in Neurodegenerative Disease Research, Santa Fe, NM, February 4–7, 2013*, Keystone Symposia on Molecular and Cellular Biology, Silverthorne, CO
34. Otvos, L., Jr., Feiner, L., Lang, E., Szendrei, G. I., Goedert, M., and Lee, V. M. (1994) Monoclonal-antibody PHF-1 recognizes tau protein phosphorylated at serine residue 396 and 404. *J. Neurosci. Res.* **39,** 669–673
35. Lee, V. M., Balin, B. J., Otvos, L., Jr., and Trojanowski, J. Q. (1991) A68- -a major subunit of paired helical filaments and derivatized forms of normal Tau. *Science* **251,** 675–678
36. Lewis, J., Dickson, D. W., Lin, W.-L., Chisholm, L., Corral, A., Jones, G., Yen, S.-H., Sahara, N., Skipper, L., Yager, D., Eckman, C., Hardy, J., Hutton, M., and McGowan, E. (2001) Enhanced neurofibrillary degeneration in transgenic mice expressing mutant Tau and APP. *Science* **293,** 1487–1491
37. Wang, M. S., Boddapati, S., and Sierks, M. R. (2009) Cyclodextrins promote protein aggregation posing risks for therapeutic applications. *Biochem. Biophys. Res. Commun.* **386,** 526–531
38. Hooper, C., Killick, R., and Lovestone, S. (2008) The GSK3 hypothesis of Alzheimer's disease. *J. Neurochem.* **104,** 1433–1439
39. Greenberg, S. G., Davies, P., Schein, J. D., and Binder, L. I. (1992) Hydrofluoric acid-treated tau-PHF proteins display the same biochemical-properties as normal tau. *J. Biol. Chem.* **267,** 564–569
40. Hawasli, A. H., Benavides, D. R., Nguyen, C., Kansy, J. W., Hayashi, K., Chambon, P., Greengard, P., Powell, C. M., Cooper, D. C., and Bibb, J. A. (2007) Cyclin-dependent kinase 5 governs learning and synaptic plasticity via control of NMDAR degradation. *Nat. Neurosci.* **10,** 880–886
41. Li, T., Hawkes, C., Qureshi, H. Y., Kar, S., and Paudel, H. K. (2006) Cyclin-dependent protein kinase 5 primes microtubule-associated protein Tau site-specifically for glycogen synthase kinase 3β†. *Biochemistry* **45,** 3134–3145
42. Lucas, J. J., Hernández, F., Gómez-Ramos, P., Morán, M. A., Hen, R., and Avila, J. (2001) Decreased nuclear β-catenin, tau hyperphosphorylation and neurodegeneration in GSK-3β conditional transgenic mice. *EMBO J.* **20,** 27–39

Diaminothiazoles Modify Tau Phosphorylation and Improve the Tauopathy in Mouse Models

Xuemei Zhang, Israel Hernandez, Damien Rei, Waltraud Mair, Joydev K. Laha, Madison E. Cornwell, Gregory D. Cuny, Li-Huei Tsai, Judith A. J. Steen and Kenneth S. Kosik

J. Biol. Chem. 2013, 288:22042-22056.
doi: 10.1074/jbc.M112.436402 originally published online June 4, 2013
